

Analytical, numerical and experimental investigation of Luneburg lens system for directional cloaking

C. Babayiğit^{1,*}, Aydın S. Evren², E. Bor^{1,2}, H. Kurt¹ and M. Turdnev²

¹Department of Electrical and Electronics Engineering, TOBB University of Economics and Technology, Ankara 06560, Turkey

²Department of Electrical and Electronics Engineering, TED University, Ankara 06420, Turkey

*e-mail: cbabayigit@etu.edu.tr

Abstract

In this study, the design of a directional cloaking based on the Luneburg lens system is proposed and its operating principle is experimentally verified. The cloaking concept is analytically investigated via geometrical optics and numerically realized with the help of finite-difference time-domain method. In order to benefit from its unique focusing/collimating characteristic of light, the Luneburg lens is used. We show that by the proper combination of the Luneburg lenses in an array form, incident light bypasses the region between junctions of the lenses, i.e., “dark zone”. Hence, direct interaction of object with propagating light is prevented if one places an object to be cloaked. This effect is used for hiding an object which is made of perfectly electric conductor material. In order to design an implementable cloaking device, the Luneburg lens is discretized into a photonic crystal structure having gradually varying air cylindrical holes in a dielectric material by using Maxwell-Garnett effective medium approximations. Experimental verifications of the designed cloaking structure are performed at microwave frequencies at around of 8 GHz. The proposed structure is fabricated by 3D printing of dielectric polylactide material and the brass metallic alloy is utilized in place of the perfectly electric conductor material in microwave experiments. A good agreement between numerical and experimental results is found.

I. INTRODUCTION

In the field of optics, realization of optical cloaking effect has been an attractive topic that initiated by the pioneering works based on transformation optics (TO) [1–3]. Here, TO simply bends the coordinate system to efficiently manipulate the direction of light propagation [4–6]. Since optical cloaking can be defined as the concealment of an object from incident wave by bending and stretching the coordinate structures, it is not a feasible procedure that requires unnatural materials with anisotropic, spatially varying permittivity and permeability values [7]. Nevertheless, the metamaterials can provide this feature [8], but the realization of these structures is a challenging issue due to dimensions much smaller than the wavelength. In addition, the cloaking effect obtained by using TO approach is narrowband and inherently lossy which is undesired for optical applications. Hence, these listed difficulties force the researchers to look for alternative solutions on the cloaking phenomenon.

In this regard, along with TO, several new methods have been introduced to obtain optical invisibility effect. Carpet cloaking, also known as ground-plane cloak, is an approach for hiding objects under specified refractive index layer made of isotropic, low-loss and dielectric material [9–13]. Another approach is suppression of scatterings due to cloaked objects by using generalized Hilbert transforms to adapt the scattering response of hiding object [14,15]. Moreover, Kramers-Kronig relations have been presented to minimize back scattering of waves which leads to optical cloaking [16]. Recently, an interesting approach based on metamaterials and optical neutrality is proposed to provide the invisibility without evoking cloaking [17]. Last but not least, the idea of using optimization approach to obtain cloaking effect shows promising results [18–21]. Here, the optimization methods search for possible designs of cloaking structures in accordance with a specific objective function. Furthermore, experimental verifications at microwave frequency regime of cloaking designs based on optimization methods were reported in Refs. [22] and [23]. In addition to these studies, focusing effect is also used for creating invisible regions both in ray and wave optics [24,25]. Moreover, the graded index (GRIN) optics can be considered as a powerful tool for efficient

light manipulation. The GRIN medium efficiently bends the light to follow curved trajectories because of the gradual change in refractive index along the radial or axial directions [26–28]. For this reason, GRIN medium provides an opportunity to obtain curved light without curved interfaces for the optical phenomena such as focusing/collecting, diverging/spreading [29]. In this regard, the conceptual studies on optical cloaking by using GRIN optics are reported lately in [30–32].

In this study, we proposed the idea of using GRIN optics concept to cloak a highly scattering cylindrical object made of perfectly electric conductor (PEC) material. In particular, the combination of GRIN Luneburg lenses is used for optical hiding purpose. The ray transfer analysis of Luneburg lenses as a cloaking system is analytically derived via geometrical optics. Next, in order to design realizable cloaking device, the continuous GRIN Luneburg lens is discretized as GRIN photonic crystal (PC) structure having varying radii of air cylindrical holes in a dielectric slab by using Maxwell-Garnett approximations, i.e., effective medium theory (EMT). As a dielectric host material, polylactide (PLA) thermoplastic having effective permittivity of $\epsilon_{\text{PLA}}=2.4025$ is employed. The numerical analysis of the optical cloaking effect is conducted by three-dimensional (3D) finite-difference time-domain (FDTD) method. Moreover, designed GRIN PC Luneburg cloaking system is fabricated by using 3D printing technology and experimental verification of numerical results are performed at microwave frequencies. It should be noted that the preliminary data of this study without analytical and experimental proof was presented in an international conference [33].

II. A RAY THEORY MODEL OF THE CLOAKING BY LUNEBURG LENS

In this section, geometrical optics is used to examine the mathematical explanation of the light behavior in the Luneburg lens which is a spherical GRIN medium where the refractive index varies radially starting from center to the outer boundary of the lens [34]. The general index distribution of Luneburg lens can be defined as follows:

$$n(r) = n_0 \sqrt{2 - \left(\frac{r}{R}\right)^2}, \quad (1)$$

where n_0 is the refractive index of the surrounding space of the lens (in our case surrounding space considered to be air, so $n_0=1$), R is the radius of the lens and r is the radial polar coordinate within the lens region. In Figs. 1(a) and 1(b), schematic representation of a Luneburg lens and corresponding refractive index distribution along the polar axis (the cross-section through the lens is shown by dashed line as an inset in Fig. 1(a)) are given, respectively. Due to the radial symmetry and Luneburg lens refractive index distribution characteristic, incoming parallel rays are focused to the point at the opposite side. Also, the rays diverging from a single point located on the lens surface are collimated into parallel rays on its back surface. This special characteristic of the Luneburg lens can be analyzed by using geometrical optics based on Fermat's principle [35]. For this purpose, quasi two-dimensional (2D) ray solution is conducted by using the 2D media which has the same index distribution characteristic with Luneburg lenses [36]. By combining the Fermat's principle with the Lagrangian optics, ray tracing equation for a single Luneburg lens can be represented as follows [37–39]:

$$y(x) = \frac{[2x_0 y_0 + R^2 \sin(2\theta)]x}{2x_0^2 + R^2 (1 + \cos(2\theta))} + \frac{\sqrt{2}R\sqrt{R^2 (1 + \cos(2\theta)) + 2x_0^2 - 2x^2} (y_0 \cos(\theta) - x_0 \sin(\theta))}{2x_0^2 + R^2 (1 + \cos(2\theta))}, \quad (2)$$

where $y(x)$ is a ray trajectory function with respect to position x , R is the radius of the lens, (x_0, y_0) are initial ray positions and θ is incidence angle of the ray. Detailed analytical derivation of Eq. (2) is provided in Supplemental Material of the study. The ray trajectory equation is simplified by considering the parallel incident rays where incidence angle $\theta = 0^\circ$:

$$y(x) = \frac{y_0(x_0 x + R\sqrt{R^2 + x_0^2 - x^2})}{x_0^2 + R^2}. \quad (3)$$

At the back surface of the lens, propagated light rays encounter with the free space and, as a result of Snell's law, they refract with exit angles. The exit angles of the rays can be obtained from the slope information of the ray trajectory. Hence by taking derivative of Eq. (2) with respect to x , propagating rays leave the lens with angles of departure according to the following equation:

$$\dot{y}(x) = \frac{R^2 \sin(2\theta) + 2x_0 y_0}{2x_0^2 + R^2(1 + \cos(2\theta))} + \frac{2\sqrt{2}Rxy_0(\sin(\theta) - \cos(\theta))}{[2x_0^2 + R^2(1 + \cos(2\theta))]\sqrt{R^2(1 + \cos(2\theta)) - 2x^2 + 2x_0}}. \quad (4)$$

The ray trajectories are calculated by using Eqs. (2)–(4) and the corresponding ray pictures are plotted for a single, double and quadruple combinations of Luneburg lenses in Figs. 1(c), 1(d) and 1(e), respectively. The focusing property of the Luneburg lens, where the incoming parallel rays focused into a single point, is proved by the solution of the ray tracing equation and the obtained result is given in Fig. 1(c). In addition, by adjoining two lenses, re-transformation of the focused light into the plane wave can be observed in Fig. 1(d). In Fig. 1(d), one can see the “ray free” regions (upside and underside regions where two lenses are connected) that are not affected by the incoming ray. From this point of view, as a next step, via the two-by-two arrangement of the Luneburg lenses, a quadruple lens system can be composed. Fig. 1(e) illustrates the ray picture of the quadruple lens system. Here, one can see an isolated region from the incoming rays at the center of the quadruple lens system, which is called as “dark zone”. Thus, this region can be used to electromagnetically hide an object from an incident wave.

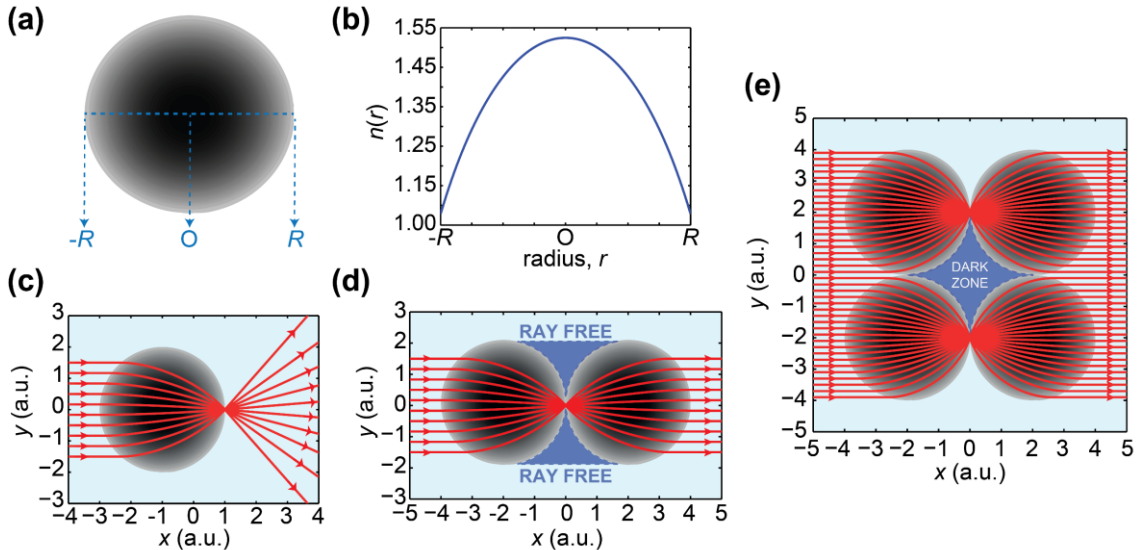


FIG. 1. (a) Schematic representation of Luneburg lens. (b) Luneburg lens refractive index profile with respect to radius. Ray tracing of a parallel rays through (c) a single Luneburg lens, (d) double Luneburg lens system, and (e) quadruple Luneburg lens system.

In summary, Fig. 1(e) exhibits the stunning potential of the quadruple Luneburg lens system that may efficiently cloak an object. In order to design a more realistic cloaking device in accordance with cloaking concept presented in ray theory analysis, the realistic design approach with its numerical analysis is given in the following sections.

III. DESIGN APPROACH AND NUMERICAL ANALYSIS

In this study, the ray theory of light-ray propagation through the Luneburg lens system is presented to provide the concept of directional cloaking. Even though geometrical optics gives some insights about operation principle of the proposed design, it is also necessary to analyze the performance of the cloaking system by conducting FDTD method for the analysis of light matter interaction.

In general, the fabrication the continuous GRIN media with the desired index distribution can be considered as a challenging task due to fabrication limitations. In order to overcome these difficulties, the PC structures are widely used for the approximation of continuous GRIN media via implementation of EMT. There are several methods to transform continuous GRIN medium to GRIN PC medium, such as appropriate arrangement of the radii of dielectric rods/air holes, adjustment of spatial distances between PC rods and infiltration of PC air holes with different substances having different refractive indices. The main objective of these approaches is to design an inhomogeneous medium with the desired index profile by gradual change of filling factors of elementary PC cells [40]. In the presented study, in order to discretize continuous GRIN Luneburg lens, the Maxwell-Garnett EMT is employed. From the Maxwell-Garnett EMT [41], the equation of the effective permittivity for transverse electric (TE) wave polarization can be expressed as follows:

$$\epsilon_{eff} = \epsilon_{host} + \frac{2f\epsilon_{host}(\epsilon_{air} - \epsilon_{host})}{2\epsilon_{host} + (1-f)(\epsilon_{air} - \epsilon_{host})}, \quad (5)$$

where ϵ_{host} and ϵ_{air} are the permittivity values of the host media and air holes, respectively, while $f=\pi r^2/(a^2)$ represents the dielectric filling ratio and r being the radius of the air hole. Finally, the variation formula of radii of air holes for TE polarization r_{TE} can be expressed as follows:

$$r_{TE} = a \sqrt{\frac{(\epsilon_{host} - n(x, y)^2)(\epsilon_{host} + \epsilon_{air})}{\pi(\epsilon_{host} + n(x, y)^2)(\epsilon_{host} - \epsilon_{air})}}, \quad (6)$$

where “ a ” is the lattice constant and $n(x, y)$ is the refractive index function of Luneburg lens. By using (1) and (6), one can design the square lattice GRIN PC Luneburg lens for the desired host media.

In order to design the proposed cloaking concept by considering fabrication and characterization facilities, the host media is selected as PLA material. The permittivity of PLA material was selected as $\epsilon_{PLA}=2.4025$ in accordance with the Nicolson-Ross and Weir method [42] for microwave regime. The schematic view of the designed GRIN PC Luneburg lens is presented in Fig. 2(a) with corresponding structural parameters. Moreover, the PC unit cells having air holes with maximum and minimum radii are given as insets in the same figure plot where $r_{max}=0.48a$ and $r_{min}=0.17a$, respectively. Corresponding 3D view of refractive index profile is shown in Fig. 2(b) where gradual variation of index values occurs between 1.13 and 1.49. Here, to define index profile, the limits of operating wavelengths should be validated in accordance with EMT. As it is well known, the EMT is valid in the long-wavelength limit where the dielectric constituents can be averaged over the dielectric unit cell as an isotropic effective index. In order to define that long-wavelength limit, where application of EMT is valid, the dispersion relations of constituent PC unit cells (air holes drilled in PLA dielectric slab) are calculated by exploiting plane wave expansion (PWE) method [43]. The

calculated dispersion diagrams of the first band in the ΓX direction for the largest and smallest air holes radii of PC unit cells are depicted in Fig. 2(c) where the direction of ΓX is presented by giving irreducible Brillouin zone. As can be deduced from this figure, the dispersion relation is nearly linear in the normalized frequency interval between $a/\lambda=0.01$ and $a/\lambda=0.30$. By using the slope information of the corresponding band diagrams, effective refractive index curves are extracted and depicted in Fig. 2(d). Here, effective refractive index values are nearly constant (linear) in the normalized frequency interval of $a/\lambda=0.01$ and $a/\lambda=0.25$. Hence, operating within this normalized frequency range ensures the validity of EMT.

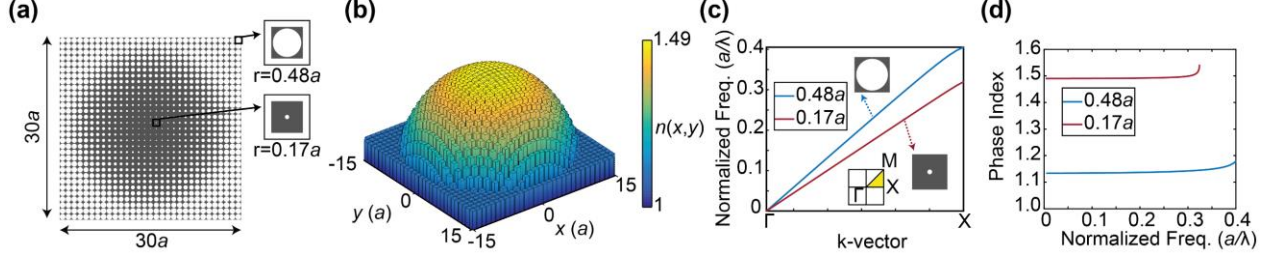


FIG. 2. (a) Schematic representation of designed Luneburg GRIN PC lens and its (b) stair-step (discrete) version of the index profile for frequency interval of $a/\lambda=0.01$ and $a/\lambda=0.25$. (c) The dispersion diagram of the first band along the Γ -X direction is shown. (d) Phase index curves corresponding to each dispersion bands shown in (c).

The main purpose of this study is to design a cloaking device which utilizes a Luneburg lens system. The concept of the proposed cloaking approach is explained in the ray-theory part of the study. If we consider plane wave propagation through proposed lens system, one can observe that the light inherently bends around the “dark zone” because of the strong focusing effect. Hence, this zone is inherently bypassed by the light waves so that this effect can be used for hiding an object from the electromagnetic light waves. This region can be considered as an “*electromagnetically hidden*” region so that one can design a directional cloaking device for the concealment of an object from the electromagnetic waves, using the quadruple lens system as shown in Fig. 1(e). In this regard, the GRIN PC Luneburg lens, which is designed and presented in Fig. 2(a), can be considered as a composing part for the proposed quadruple lens system. Here, GRIN PC Luneburg lens in Fig. 2(a) is scaled by adjusting the lattice constant as $a=2.87$ mm in order to operate in the microwave regime. It is important to note that fabrication of the cloaking device and its experimental verification are also considered while fixing the lattice constant.

Figure 3, in general, presents the conceptual design of the proposed cloaking device with its effective refractive index profile. As it can be seen from Fig. 3(a), cloaking device is constructed by the junction of the four GRIN PC Luneburg lenses. An air hole is intentionally reamed at the center of the cloaking structure to place the object that considered for concealing. Here, the position of the air hole is arranged in a way that it overlaps with the emerging “dark zone” shown in Fig. 1(e). The designed cloaking device has width and length equal to 172 mm as shown in Fig. 3(b) and the slab thickness is fixed to $h=24$ mm. In Figs. 3(a) and 3(b), the arrows indicate the direction of wave propagation. As a cloaking object, the cylindrical shaped PEC material with diameter of 36 mm and height of 24 mm is used. The corresponding 3D view of effective refractive index profile of the proposed cloaking system is presented in Fig. 3(c) where the “dark zone” is defined by the dashed circle at the center of the profile.

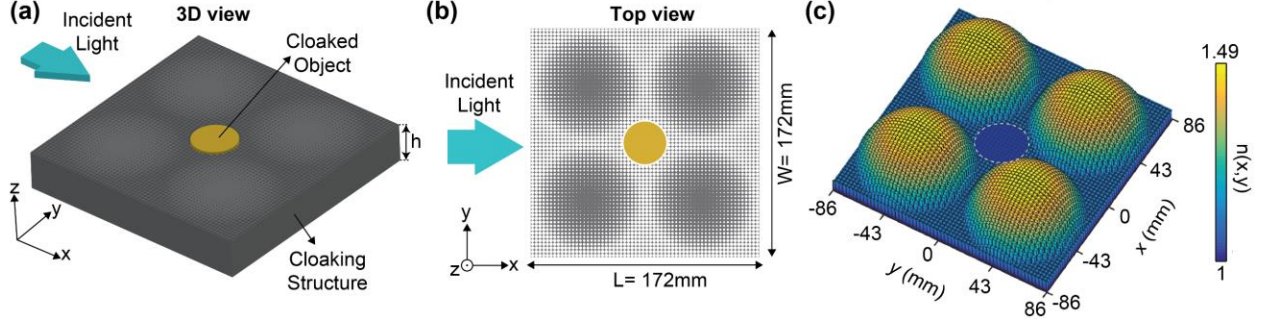


FIG. 3. (a) Three-dimensional and (b) top views of the designed cloak. (c) The stair-step (discrete) effective index profile of the proposed cloaking system.

In order to numerically analyze the cloaking performance of the proposed structure, FDTD method is employed. In the FDTD simulations, we used plane wave source to excite the cylindrical PEC object to analyze its scattering characteristics in free-space medium. It is important to note that PEC material is a conductive material with infinite conductivity, which results in 100% reflection and 0% absorption characteristic against an incident electromagnetic field. For this reason, to clarify the cloaking performance of the proposed structure, PEC material is used through the numerical analyses. The TE polarized plane wave source operating at microwave frequency of 8 GHz (this frequency is obtained by transforming normalized frequency of $a/\lambda=0.08$ to 8 GHz) is utilized to illuminate the cloaking structure. It should be noted that, for TE polarization, the electric field components are along the xy -plane (E_x, E_y) and the magnetic field (H_z) is perpendicular to the xy -plane. The magnetic field (H_z) and phase (ϕ) distributions for the cases when only PEC structure was placed in free-space and the cloaking structure covered the PEC object are calculated and given in Figs. 4(a) and 4(b), respectively. As can be clearly observed from magnetic field distribution in Fig. 4(a) (top), incident plane wave is strongly scattered by PEC object. Also, the corresponding phase distribution gives evidence of the wavefronts deterioration as shown in Fig. 4(b) (top). On the other hand, when the PEC is covered by the designed cloaking structure, the scatterings are substantially suppressed where the PEC region remains isolated. Here, the magnetic field and phase profiles stay undeformed at the output of the structure as can be seen in Fig. 4(a) (bottom) and 4(b) (bottom), respectively. Thus, plane wave propagation nature of the incident light is mostly conserved even a PEC material is placed inside the structure.

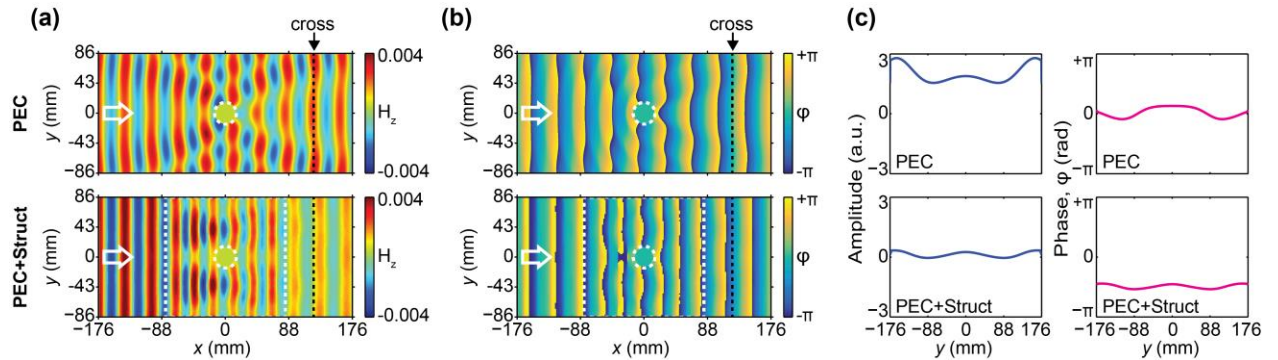


FIG. 4. The numerically calculated (a) magnetic field and (b) phase distributions are given for the cases of PEC placed in free-space (top) and PEC is surrounded by cloaking structure (bottom). The arrows indicate the direction of propagation for the incident plane waves. (c) The plotted amplitude and phase profiles are calculated at the positions denoted by dashed lines in (a) and (b).

In order to quantitatively analyze the performance of the cloaking device, cross-sectional amplitude and phase profiles are calculated at the positions (dashed lines in Figs. 4(a) and 4(b)) and shown in Fig. 4(c). As can be seen from this figure, the PEC object highly scatters the incident wave which results in high

fluctuations of cross-sectional amplitude and phase profiles. On the other hand, emerged fluctuations in the field amplitude and phase are considerably smoothed by the cloak introduced to the PEC object as shown in Fig. 4(c) (bottom). One can conclude that the decrement of fluctuations in cross-sectional profiles indicates the formation of plane waves at the output that replicates the incident one. This effect demonstrates the cloaking ability of the proposed quadruple Luneburg lens system. It should also be pointed out that all the numerical analyses, which were obtained by using the ray theory, are in accordance with the FDTD simulations.

IV. EXPERIMENTAL VERIFICATION OF THE NUMERICALLY ANALYZED CLOAKING EFFECT IN THE MICROWAVE REGIME

The experimental verification of cloaking concept via quadruple Luneburg lens system is achieved by performing experiments at microwave frequencies. In this regard, the designed cloaking structure is fabricated by 3D printing of PLA material. Here, as aforementioned, the permittivity of PLA material is equal to $\epsilon_{\text{PLA}}=2.4025$. In order to make a realistic experiment, the cylindrical brass object was used for experiments in place of PEC object. Here, brass metallic object is a mixture of copper and zinc, exhibits strong scattering characteristics at the microwave frequencies of interest. During the experimental process, we used Agilent E5071C ENA vector network analyzer to generate and detect microwaves. The fabricated cloaking structure is excited by using horn antenna with operating bandwidth of 6 GHz – 12 GHz placed in front of it. Since the horn antenna radiates a Gaussian profiled wave, it was located at an adequate distance away from the cloaking structure to obtain plane wave-like propagating waves. Moreover, a monopole antenna placed on a motorized stage was utilized to measure the magnetic field (H_z) and phase (ϕ) distributions at the scanning field behind the fabricated cloaking structure. In order to measure the magnetic field and phase distributions, the monopole antenna was moved with 2 mm steps along both x -axis and y -axis. It should be noted that the scanning field is on a level with the half of the thickness of cloaking structure in z -direction. The complete schematic representation of experimental setup is depicted in Fig. 5(a). Furthermore, the photographic view of fabricated cloaking structure with cylindrical brass object placed inside it is given in Fig. 5(b) where a coin is placed for visual comparison of dimensions of the structure and brass object.

Initially, we measured the scatterings due to the brass object. Therefore, we positioned the brass object in front of the horn antenna, and then scanned the magnetic field and phase distributions behind it via the monopole antenna. Next, we placed the cloaking structure with brass object at a sufficient distance away from the horn antenna and measured the magnetic field and phase distributions behind the cloaking structure. The corresponding magnetic field and phase distributions were measured for incident wave with frequency of 8 GHz and represented in Figs. 5(c) and 5(d), respectively. As can be seen from the top image of Fig. 5(c), the incident light is strongly scattered and it is divided into two branches by making a shadow at the back surface of the brass object. On the other hand, the cloaking structure reduces the scatterings (almost no sign of existence of the brass object) and one can conclude that the cloaking structure is managed to equalize the magnetic field amplitude along the y -axis by altering the scattered fields due to brass object. In order to give complete picture of cloaking, the measured phase distributions are given in top and bottom images of Fig. 5 (d), respectively, for the brass object alone and cloaking structure with brass object inside it. Here, the brass object scatters the incident wave to have curved wavefronts behind it, while the cloaking structure reshapes the propagated fields to have plane wavefronts. The dashed lines in Figs. 5(c) and 5(d) indicate the positions of cross-sectional profiles of magnetic field and phase distributions. The corresponding cross-sectional profiles are plotted in Fig. 5(e) to demonstrate the scatterings of brass object and cloaking effect of the quadruple Luneburg lens system. As can be seen from the plots in Fig. 5(e), the fluctuations in amplitude and phase profiles are reduced when the cloaking structure introduced to cloak the brass object.

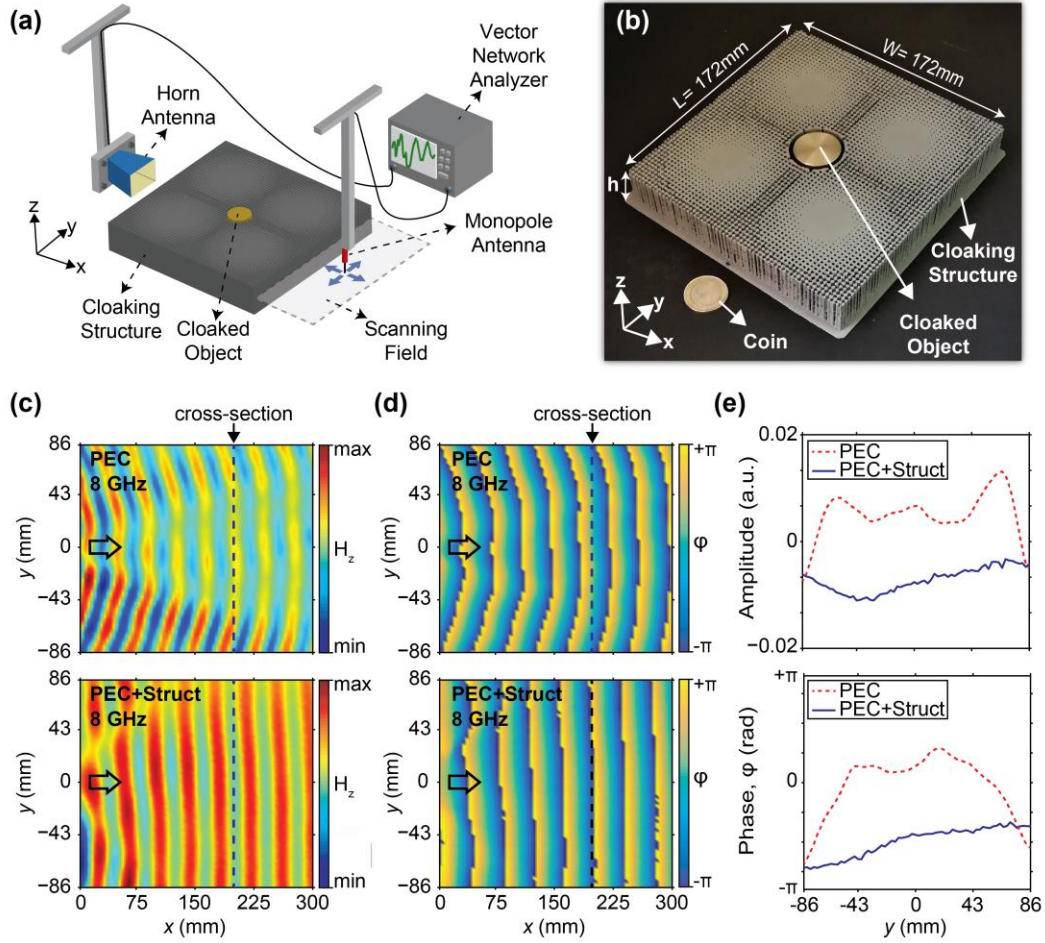


FIG. 5. (a) Schematic representation of the experimental setup. (b) The photographic view of fabricated cloaking structure and cylindrical brass cloaked object. A coin is shown for comparison of structural dimensions. (c) The measured magnetic field (H_z) and (d) phase (ϕ) distributions in the scanning field at frequency of 8 GHz for experiment cases when brass object alone (PEC) and cloaking structure with brass object inside (PEC+Struct.). The arrows denote the direction of incident wave and the dashed lines indicate the positions of cross-sectional profiles. (e) The corresponding cross-sectional profiles of magnetic field amplitude and phase.

V. CONCLUSION

In summary, directional cloaking ability of the proposed quadruple Luneburg lens system is presented. The ray analysis of a single Luneburg lens is examined which is later adapted to the formation of double and quadruple Luneburg lenses. As a result, electromagnetically hidden space is emerged in the middle of a quadruple Luneburg lens system which is an adequate region for optical cloaking of highly scattering object such as PEC materials. In order to enable the feasibility of refractive index distribution of a Luneburg lens, Maxwell-Garnett EMT is applied by inserting air holes with gradually varying radii on a dielectric slab which results in a GRIN PC Luneburg lens. The host dielectric material is selected as PLA with permittivity of $\epsilon_{\text{PLA}}=2.4025$ and the EMT approximations are performed via PWE method which is discussed in detail. Further, cloaking of cylindrical PEC object by the quadruple GRIN PC Luneburg lens system is analyzed by employing FDTD method where the system is excited by a TE polarized plane wave source. According to the numerical results, the designed system is able to cloak the object and reproduce the plane wave aspects of the incident wave at the output area. Additionally, the proposed Luneburg lens system is fabricated via 3D printing technology and microwave experiments are performed at around the frequency

of 8 GHz for the verification of analytical solutions and numerical calculations of directional cloaking effect. During the experiments, brass alloy is preferred in substitution for the PEC material and it is observed that the printed-out lens system managed to suppress the scatterings due to highly scattering brass object. As a result, we designed, fabricated, and both numerically and experimentally validated the proposed cloaking concept of the quadruple Luneburg Lens system. The designed structure can be a good solution candidate for optical cloaking from the incident light in a defined propagation direction. One can increase the numbers of Luneburg lenses to realize even larger arrays to hide multiple objects.

APPENDIX A: DERIVATION OF RAY TRAJECTORY EQUATION

The optical path length of a ray in inhomogeneous medium between points A and B can be defined as follows [36,37]:

$$OPL = \int_A^B n(r) ds, \quad (A7)$$

where $n(r)$ corresponds to refractive index function, which varies with position, and the differential length is expressed as $ds = \sqrt{dr^2 + r^2 d\phi^2}$ in polar coordinates. Since the refractive index distribution of the

Luneburg lens is a function of r , so differential length ds can be rewritten as $ds = \sqrt{1 + r^2 \left(\frac{d\phi}{dr}\right)^2} dr$. Let

$\frac{d\phi}{dr} = \dot{\phi}$, then the equation (A1) becomes:

$$OPL = \int_A^B n(r) \sqrt{1 + r^2 \dot{\phi}^2} dr. \quad (A8)$$

Here, the shortest path that is followed by a light-ray according to Fermat Principle can be obtained by the minimization of the integral of (A2). In this regard, to obtain derivative of (A2), the Euler-Lagrange equation can be used where Lagrangian is $L(\phi, \dot{\phi}, r) = n(r) \sqrt{1 + r^2 \dot{\phi}^2}$ [36,39]:

$$\frac{d}{dr} \frac{\partial L}{\partial \dot{\phi}} = \frac{\partial L}{\partial \phi}. \quad (A9)$$

Taking into consideration that the structure is invariant in the ϕ direction, the derivative of $\partial L / \partial \phi$ becomes equal to zero. Then, the left-hand side of (A3), $\partial L / \partial \dot{\phi}$, should be a constant value, since $\frac{d}{dr} \frac{\partial L}{\partial \dot{\phi}} = 0$. Taking the derivative of the Lagrangian equation with respect to the $\dot{\phi}$ and equalizing it to constant C_1 , we obtain:

$$\frac{\partial L}{\partial \dot{\phi}} = \frac{n(r)r^2}{\sqrt{1 + r^2 \dot{\phi}^2}} \dot{\phi} = C_1. \quad (A10)$$

Next, the nonlinear differential equation (A4) can be rewritten by replacing $\dot{\phi}$ with $d\phi/dr$:

$$\frac{n(r)r^2}{\sqrt{1 + r^2 \left(\frac{d\phi}{dr}\right)^2}} \frac{d\phi}{dr} = C_1. \quad (A11)$$

Then, as a step to reach ray trajectory $r(\varphi)$, one should solve (A5) for $d\varphi$ and integrate both sides as follows:

$$\varphi = \frac{1}{2} \sin^{-1} \left[\frac{r^2 - \frac{C_1^2 R^2}{n(r)^2}}{r^2 \sqrt{1 - \frac{C_1^2}{n(r)^2}}} \right] - \beta, \quad (\text{A12})$$

where R is the radius of the lens. Next, by solving (A6) with respect to r , the ray trajectory equation can be found as follows:

$$r(\varphi) = \frac{C_2 R}{\sqrt{1 - \sqrt{1 - C_2^2} \sin(2(\varphi + \beta))}}, \quad (\text{A13})$$

where $C_2 = C_1^2 / n(r)^2$ and β are constants. Since we are dealing with ray propagation in Cartesian coordinates, it is logical to transfer the ray trajectory formula (A7) to the Cartesian coordinate [34,37]:

$$(1 - T \sin(2\beta))x^2 + (1 + T \sin(2\beta))y^2 - 2T \cos(2\beta)xy + (T^2 - 1)R^2 = 0. \quad (\text{A14})$$

T and β are constant numbers and to find them the boundary conditions which are related with the initial position and the initial incident angle should be used. The first boundary condition depends on the initial position of the ray, where it enters the lens. Let place the center of lens to the position $[x=0, y=0]$. If the angle of incidence is θ , then the initial ray position is expressed as $[x_0 = -R \cos(\theta), y_0 = -R \sin(\theta)]$. By replacing x and y with the position of initial point in the (A8), one can solve (A8) with respect to constant number T as follows:

$$T = \sin(2\beta + 2\theta). \quad (\text{A15})$$

The second boundary condition comes from the $dy/dx = \tan(\theta)$ relation and by taking derivative of the (8) with respect to x , and then solving it for T by setting $x = x_0$ and $y = y_0$:

$$T = \frac{x_0 + y_0 \tan(\theta)}{\tan(\theta)[x_0 \cos(2\beta) - y_0 \sin(2\beta)] + [x_0 \sin(2\beta) + y_0 \cos(2\beta)]}. \quad (\text{A16})$$

Here, to find the analytical expression for β , (A9) and (A10) are combined and solved for β as follows:

$$\beta = \frac{1}{2} (\tan^{-1} \left(\frac{x_0}{y_0} \right) - \theta). \quad (\text{A17})$$

Then, if the β is inserted to (A9), both T and β constants will be represented in terms of the initial positions $[x_0, y_0]$ and the incidence angle θ :

$$T = \sin(\tan^{-1} \left(\frac{x_0}{y_0} \right) + \theta). \quad (\text{A18})$$

After finding the constants T and β , (A8) can be solved for y by using the quadric formula as follows:

$$y = \frac{T \cos(2\beta)x}{(1 - T \sin(2\beta))} + \frac{\sqrt{(T \cos(2\beta)xy)^2 - (1 - T \sin(2\beta))[(T^2 - 1)R^2 + (1 + T \sin(2\beta))x^2]}}{(1 + T \sin(2\beta))}. \quad (\text{A19})$$

To simplify the representation of (A13), let divide it into two components as follows:

$$A = \frac{T \cos(2\beta)x}{(1 - T \sin(2\beta))} \quad (\text{A20})$$

and

$$B = \frac{\sqrt{(T \cos(2\beta)xy)^2 - (1 - T \sin(2\beta))[(T^2 - 1)R^2 + (1 + T \sin(2\beta))x^2]}}{(1 + T \sin(2\beta))}. \quad (\text{A21})$$

Next, solve them separately, and then merge them to obtain final result. In this regard, firstly, we substitute the formulas of constants T and β to the term A as follows:

$$A = \frac{T \cos(2\beta)x}{(1 - T \sin(2\beta))} = \frac{x \sin(\tan^{-1}(x_0 / y_0) + \theta) \cos(\tan^{-1}(x_0 / y_0) - \theta)}{1 + \sin(\tan^{-1}(x_0 / y_0) + \theta) \sin(\tan^{-1}(x_0 / y_0) - \theta)}. \quad (\text{A22})$$

Then, with the help of trigonometric identities, (A16) can be further simplified to the following equation:

$$A = \frac{x \sin(\tan^{-1}(x_0 / y_0)) \cos(\tan^{-1}(x_0 / y_0))}{1 + 0.5[(1 + \cos(2\theta)) - 2 \cos^2(\tan^{-1}(x_0 / y_0))]} + \frac{0.5 \sin(2\theta)x}{1 + 0.5[(1 + \cos(2\theta)) - 2 \cos^2(\tan^{-1}(x_0 / y_0))]} \quad (\text{A23})$$

As a next step, by setting $\alpha = \tan^{-1}(x_0 / y_0)$ and using the circle equation, one can obtain definitions $\sin(\alpha) = (x_0 / R)$ and $\cos(\alpha) = (y_0 / R)$. In this sense, (A17) can be rewritten as follows:

$$A = \frac{[\sin(\alpha) \cos(\alpha) + 0.5 \sin(2\theta)]x}{1 + 0.5[(1 + \cos(2\theta)) - 2 \cos^2(\alpha)]} = \frac{x[(x_0 / R)(y_0 / R) + 0.5 \sin(2\theta)]x}{1 + 0.5[(1 + \cos(2\theta)) - 2(y_0 / R)^2]} = \frac{[2x_0 y_0 + R^2 \sin(2\theta)]x}{2x_0^2 + R^2(1 + \cos(2\theta))} \quad (\text{A24})$$

Equation (A18) is the last version of the first term A . The next goal is simplifying the second term B . For that purpose, (A15) can be rewritten as indicated below:

$$\begin{aligned} B &= \frac{\sqrt{(T \cos(2\beta)xy)^2 - (1 - T \sin(2\beta))[(T^2 - 1)R^2 + (1 + T \sin(2\beta))x^2]}}{(1 + T \sin(2\beta))} \\ &= \frac{\sqrt{(T^2 - 1)x^2 + (T^2 - 1)(-T \sin(2\beta) + 1)R^2}}{(1 + T \sin(2\beta))} \\ &= \frac{\sqrt{(T^2 - 1)(x^2 - R^2(1 + T \sin(2\beta)))}}{1 + T \sin(2\beta)} \end{aligned} \quad (\text{A25})$$

There are two important expressions in (A19) which are $(T^2 - 1)$ and $(1 + T \sin(2\beta))$. By substituting the formulas of constants T and β to these expressions, B term will be written in terms of the initial position and the initial incident angle. For that purpose, the following operations were carried out with the mentioned expressions:

$$\begin{aligned}
T^2 - 1 &= \sin(\tan^{-1}(x_0/y_0) + \theta)^2 - 1 = \sin(\alpha + \theta)^2 - 1 = \frac{1 - \cos(2\alpha + 2\theta)}{2} - 1 \\
&= \frac{-1 - (2\cos^2(\alpha) - 1)\cos(2\theta) - 2\sin(\alpha)\cos(\alpha)\sin(2\theta)}{2} \\
&= \frac{-R^2 - (2y_0^2 - R^2)\cos(2\theta) + 2x_0y_0\sin(2\theta)}{2R^2}
\end{aligned} \tag{A26}$$

$$\begin{aligned}
1 + T \sin(2\beta) &= 1 + \sin(\tan^{-1}(x_0/y_0) + \theta)\sin(\tan^{-1}(x_0/y_0) - \theta) = 1 + \sin(\alpha + \theta)\sin(\alpha - \theta) \\
&= \frac{3 + \cos(2\theta) - 2\cos^2(\alpha)}{2} = \frac{(1 + \cos(2\theta))R^2 + 2x_0^2}{2R^2}
\end{aligned} \tag{A27}$$

Then, by combining (A19), (A20) and (A21), the final version of the B term can be obtained in the simplest way as follows:

$$B = \frac{\sqrt{2}R(y_0 \cos(\theta) - x_0 \sin(\theta))\sqrt{R^2(1 + \cos(2\theta)) + 2x_0^2 - 2x^2}}{2x_0^2 + R^2(1 + \cos(2\theta))}. \tag{A28}$$

Here, the simplified version of the A and B are attained in (A18) and (A23), respectively. Finally, by merging (A18) and (A23), we obtain ray trajectory equation in Cartesian coordinate system as follows:

$$\begin{aligned}
y(x) &= \frac{[2x_0y_0 + R^2 \sin(2\theta)]x}{2x_0^2 + R^2(1 + \cos(2\theta))} + \frac{\sqrt{2}Ry_0 \cos(\theta)\sqrt{R^2(1 + \cos(2\theta)) + 2x_0^2 - 2x^2}}{2x_0^2 + R^2(1 + \cos(2\theta))} \\
&\quad - \frac{\sqrt{2}Rx_0 \sin(\theta)\sqrt{R^2(1 + \cos(2\theta)) + 2x_0^2 - 2x^2}}{2x_0^2 + R^2(1 + \cos(2\theta))},
\end{aligned} \tag{A29}$$

where $y(x)$ is a ray trajectory function with respect to position x , and R is the radius of the lens, and (x_0, y_0) are initial ray positions, and θ is incidence angle of the ray. Moreover, the exit angle, which is the angle that ray exit the lens, should be computed for the complete ray analyses. In order to determine the exit angle, the derivative of the (A23) should be taken with respect to x as follows:

$$\dot{y}(x) = \frac{R^2 \sin(2\theta) + 2x_0y_0}{2x_0^2 + R^2(1 + \cos(2\theta))} + \frac{2\sqrt{2}Rxy_0(\sin(\theta) - \cos(\theta))}{[2x_0^2 + R^2(1 + \cos(2\theta))]\sqrt{R^2(1 + \cos(2\theta)) - 2x^2 + 2x_0^2}}. \tag{A30}$$

The equations (A23) and (A24) can be used to investigate multiple configurations of Luneburg lenses. In this regard, the ray trajectories that obtained analytically by using (A23) and (A24) for distinct cases are represented in Fig. 6. In Fig. 6(a), the focusing characteristic of the Luneburg lens under the different incidence angles is observed. From the figure, one can conclude that, depending on the incidence angle of the rays, the focal point shifts on the surface of the lens. Moreover, by adjoining two, four or more lenses, specific Luneburg lens systems can be designed. Here, in Figs. 6(b) and 6(c) ray trajectories for double and quadruple lens systems are presented where the incidence angles are chosen as -10° and 10° , respectively. As can be seen from the Figs. 6(b) and 6(c), even though light is incident with an angle different from normal, the “ray free” zone is emerged.

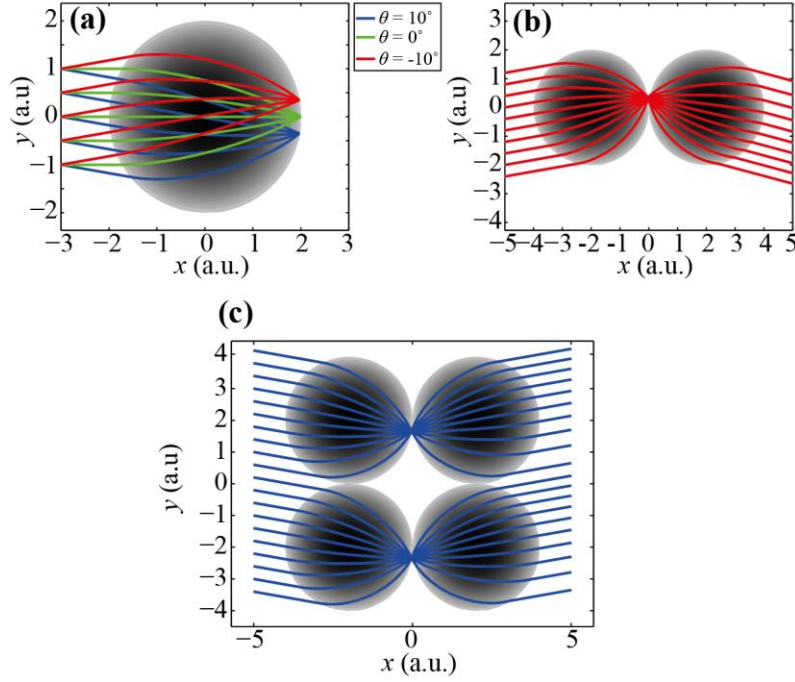


FIG. 6. Ray tracing of parallel rays through (a) a single Luneburg lens with an incidence angle $\theta = 10^\circ$, 0° and -10° , (b) double Luneburg lens system with an incidence angle $\theta = -10^\circ$, (c) quadruple Luneburg lens system with an incidence angle $\theta = 10^\circ$.

In summary, for certain initial conditions, the analyses of the several configurations of Luneburg lenses can be examined with the help of the ray trajectory equation given in (A23).

ACKNOWLEDGMENT

This work was supported by the Scientific and Technological Research Council of Turkey (TUBITAK) under Project 116F182. H. Kurt acknowledges partial support from the Turkish Academy of Sciences.

REFERENCES

- [1] U. Leonhardt, "Optical conformal mapping", *Science*, vol. 312, no. 5781, pp. 1777-1780, Jun. 2006.
- [2] J. B. Pendry, D. Schurig, and D. R. Smith, "Controlling electromagnetic fields", *Science*, vol. 312, no. 5781, pp. 1780-1782, Jun. 2006.
- [3] T. Tyc, H. Chen, C. T. Chan and U. Leonhardt, "Non-Euclidean cloaking for light waves", *IEEE J. Sel. Top. Quantum Electron.*, vol. 16, no. 2, pp. 418-426, 2010.
- [4] H. Ma, S. Qu, Z. Xu, J. Zhang, B. Chen, and J. Wang, "Material parameter equation for elliptical cylindrical cloaks", *Phys. Rev. A*, vol. 77, no. 1, 2008.
- [5] H. Chen, U. Leonhardt, and T. Tyc, "Conformal cloak for waves", *Phys. Rev. A*, vol. 83, no. 5, 2011.
- [6] M. Schmiele, C. Rockstuhl, and F. Lederer, "Strategy for cloaking of twisted domains", *Phys. Rev. A*, vol. 79, no. 5, 2009.
- [7] H. Chen, C. T. Chan, and P. Sheng, "Transformation optics and metamaterials", *Nat. Mater.*, vol. 9, pp.387-396, 2010.
- [8] W. Cai, U. K. Chettiar, A. V. Kildishev, and V. M. Shalaev, "Optical cloaking with metamaterials", *Nat. Photon.*, vol. 1, pp. 224-227, 2007.
- [9] J. Valentine, J. Li, T. Zentgraf, G. Bartal, and X. Zhang, "An optical cloak made of dielectrics", *Nat. Mater.*, vol. 8, pp. 568-571, 2009.
- [10] J. Li, and J. B. Pendry, "Hiding under the carpet: a new strategy for cloaking", *Phys. Rev. Lett.*, vol. 101, no. 20, pp. 3901-3904, 2008.

- [11] R. Liu, C. Ji, J. J. Mock, J. Y. Chin, T. J. Cui, and D. R. Smith, "Broadband ground-plane cloak", *Science*, vol. 323, no. 5912, pp. 366-369, Jan. 2009.
- [12] G. Dupont, S. Guenneau, and S. Enoch, "Electromagnetic analysis of arbitrarily shaped pinched carpets", *Phys. Rev. A*, vol. 82, no. 3, 2010.
- [13] E. Kallos, C. Argyropoulos, and Y. Hao, "Ground-plane quasicloaking for free space", *Phys. Rev. A*, vol. 79, no. 6, 2009.
- [14] Z. Hayran, R. Herrero, M. Botey, H. Kurt, and K. Staliunas, "Invisibility on demand based on a generalized Hilbert transform", *Phys. Rev. A*, vol. 98, no. 1, pp. 3822-3829, 2018.
- [15] Z. Hayran, H. Kurt, R. Herrero, M. Botey, and K. Staliunas, "All-dielectric self-cloaked structures", *ACS Photonics*, vol. 5, no. 5 pp. 2068-2073, 2018.
- [16] S. A. R. Horsley, M. Artoni, and G. C. La Rocca, "Spatial Kramers–Kronig relations and the reflection of waves", *Nat. Photon.*, vol. 9, pp. 436-439, 2015.
- [17] R. Hodges, C. Dean, and M. Durach, "Optical neutrality: invisibility without cloaking", *Opt. Lett.*, vol. 42, no. 4, pp. 691-694, 2017.
- [18] J. Andkjær, and O. Sigmund, "Topology optimized low-contrast all-dielectric optical cloak", *Appl. Phys. Lett.*, vol. 98, no. 2, p. 021112, 2011.
- [19] Y. Urzhumov, N. Landy, T. Driscoll, D. Basov, and D. R. Smith, "Thin low-loss dielectric coatings for free-space cloaking", *Opt. Lett.*, vol. 38, no. 10, pp. 1606-1608, 2013.
- [20] B. Vial, and Y. Hao, "Topology optimized all-dielectric cloak: design, performances and modal picture of the invisibility effect", *Opt. Express*, vol. 23, no. 18, pp. 23551-23560, 2015.
- [21] E. Bor, C. Babayiğit, H. Kurt, K. Staliunas, and M. Turduev, "Directional invisibility induced by a genetic optimization approach", *Opt. Lett.*, vol. 43, no. 23, pp. 5781-5784, 2018.
- [22] L. Lan, F. Sun, Y. Liu, C. K. Ong, and Y. Ma, "Experimentally demonstrated a unidirectional electromagnetic cloak designed by topology optimization", *Appl. Phys. Lett.*, vol. 103, no. 12, p. 121113, 2013.
- [23] B. Vial, M. M. Torrico, and Y. Hao, "Optimized microwave illusion device", *Sci. Rep.*, vol. 7, p. 3929, 2017.
- [24] J. S. Choi, and J. C. Howell, "Paraxial ray optics cloaking", *Opt. Express*, vol. 22, no. 24, pp. 29465-29478, 2014.
- [25] B. Vasić, and R. Gajić, "Self-focusing media using graded photonic crystals: Focusing, Fourier transforming and imaging, directive emission, and directional cloaking", *J. Appl. Phys.*, vol. 110, no. 5, p. 053103, 2011.
- [26] M. Turduev, B. Oner, I. H. Giden, and H. Kurt, "Mode transformation using graded photonic crystals with axial asymmetry", *J. Opt. Soc. Am. B*, vol. 30, no. 6, pp. 1569-1579, 2013.
- [27] B. Oner, M. Turduev, and H. Kurt, "High efficiency beam bending using graded photonic crystals", *Opt. Lett.*, vol. 38, no. 10, pp. 1688-1690, 2013.
- [28] E. Cassan, K. Do, C. Caer, D. Marris-Morini, and L. Vivien, "Short-wavelength light propagation in graded photonic crystals", *J. Light. Technol.*, vol. 29, no. 13, pp. 1937-1943, 2011.
- [29] M. Turduev, I. H. Giden, and H. Kurt, "Design of flat lens-like graded index medium by photonic crystals: exploring both low and high frequency regimes", *Opt. Commun.*, vol. 339, pp. 22-33, 2015.
- [30] B. B. Oner, M. G. Can, and H. Kurt, "Dual polarized broadband and all dielectric partial cloaking using stacked graded index structures", *Opt. Express*, vol. 22, no. 17, pp. 20457-20462, 2014.
- [31] N. A. Mortensen, O. Sigmund, and O. Breinbjerg, "Prospects for poor-man's cloaking with low-contrast all dielectric optical elements", *J. Eur. Opt. Soc. Rapid Publ.*, vol. 4, 2009.
- [32] T. Xu, Y. C. Liu, Y. Zhang, C. K. Ong, and Y. G. Ma, "Perfect invisibility cloaking by isotropic media", *Phys. Rev. A*, vol. 86, no. 4, 2012.
- [33] A. S. Evren, C. Babayiğit, E. Bor, H. Kurt, and M. Turduev, "Directional cloaking by quadruple luneburg lens system", *2018 20th International Conference on Transparent Optical Networks (ICTON)*, Bucharest, 2018, pp. 1-4.
- [34] R. K. Luneburg, and M. Herzberger. *Mathematical Theory of Optics*, Univ of California Press, 1964, pp. 182-188.

- [35] C. Gomez-Reino, M. V. Perez, and C. Bao, *Gradient-Index Optics: Fundamentals and Applications*, Springer, Berlin, 2002, p. 9.
- [36] M. Mattheakis, and G. P. Tsironis, “Extreme waves and branching flows in optical media”, in *Quodons in Mica*, Springer Series in Materials Science, 2005, pp. 425-454.
- [37] V. Lakshminarayanan, A. K. Ghatak, and K. Thyagarajan, *Lagrangian Optics*, Kluwer Academic Publishers, 2002, p. 27.
- [38] M. Kline, I. W. Kay, *Electromagnetic Theory and Geometric Optics*, Interscience, New York, 1965, p.13.
- [39] M. M. Mattheakis, G. P. Tsironis, and V. Kovanis, “Luneburg lens waveguide networks”, *J. Opt.*, vol. 14, no. 11, p. 114006, 2012.
- [40] S. Khosravi, A. Rostami, G. Rostami, and M. Dolatyari, "Midinfrared invisibility cloak design using composite optical materials", *IEEE J. Sel. Top. Quantum Electron.*, vol. 22, no. 1, pp. 134-139, 2016.
- [41] A. Sihvola, “Classical mixing approach”, in *Electromagnetic Mixing Formulas and Applications*, The Institution of Electrical Engineers, London, United Kingdom, 1999, pp. 39-52.
- [42] W. B. Weir, “Automatic measurement of complex dielectric constant and permeability at microwave frequencies”, *Proc. IEEE*, vol. 62, no. 1, pp. 33-36, 1974.
- [43] S. Johnson, and J. D. Joannopoulos, “Block-iterative frequency-domain methods for Maxwell’s equations in a planewave basis”, *Opt. Express*, vol. 8, no. 3, pp. 173-190, 2001.